2-21-2013

Biparametric Analyses of Charge Trapping in $Cd_{0.9}Zn_{0.1}Te$ Based Virtual Frisch Grid Detectors

S. K. Chaudhuri

K. J. Zavalla

R. M. Krishna

K. C. Mandal
University of South Carolina - Columbia, mandalk@engr.sc.edu

Publication Info

Published in *Journal of Applied Physics*, Volume 113, Issue 7, 2013, pages 074504-1-074504-6.

Chaudhuri, S. K., Zavalla, K. J., Krishna, R. M., & Mandal, K. C. (21 February 2013). Biparametric analyses of charge trapping in $Cd_{0.9}Zn_{0.1}Te$ based virtual Frisch grid detectors. *Journal of Applied Physics*, 113(7), #074504.
http://dx.doi.org/10.1063/1.4793268
http://scitation.aip.org/content/aip/journal/jap/113/7/10.1063/1.4793268

Biparametric analyses of charge trapping in Cd0.9Zn0.1Te based virtual Frisch grid detectors

Sandeep K. Chaudhuri, Kelvin J. Zavalla, Ramesh M. Krishna, and Krishna C. Mandal

Citation: Journal of Applied Physics **113**, 074504 (2013); doi: 10.1063/1.4793268
View online: http://dx.doi.org/10.1063/1.4793268
View Table of Contents: http://scitation.aip.org/content/aip/journal/jap/113/7?ver=pdfcov
Published by the AIP Publishing

Biparametric analyses of charge trapping in $Cd_{0.9}Zn_{0.1}Te$ based virtual Frisch grid detectors

Sandeep K. Chaudhuri, Kelvin J. Zavalla, Ramesh M. Krishna, and Krishna C. Mandal[a)]
Department of Electrical Engineering, University of South Carolina, Columbia, South Carolina 29208, USA

(Received 20 December 2012; accepted 8 February 2013; published online 21 February 2013)

Detector grade $Cd_{0.9}Zn_{0.1}Te$ (CZT) single crystals were grown from zone refined Cd, Zn, and Te (~7 N) precursor materials, using a tellurium solvent method. Detectors with virtual Frisch grid configuration were fabricated using these crystals. I-V measurements revealed low leakage currents at room-temperature, ~11 nA for one such detector D1 and ~8 nA for another detector D2 at 1100 V. The spectroscopic performances of the two CZT virtual Frisch grid detectors have been evaluated and compared for high energy gamma ray detection. Detector D1 showed a well-resolved pulse-height spectrum with an energy resolution of ~1.6% for the 662 keV gamma rays. Detector D2 also showed a distinct 662 keV peak but with a broader pulse-height distribution. A digital biparametric correlation study of the depth of interaction and energy deposited by the 662 keV gamma rays was carried out. A different kind of correlation pattern from that observed normally for hole trapping was noticed in the case of detector D2. Correlation of results from thermally stimulated current measurement studies suggested that the anomalous biparametric correlation pattern was due to the trapping of holes but modified by the virtual Frisch grid effect. The results also suggested that the effect of electron trapping could not be ruled out either. Finally, a digital correction scheme was applied to recover the ^{137}Cs spectrum from the effect of charge loss. © *2013 American Institute of Physics*. [http://dx.doi.org/10.1063/1.4793268]

I. INTRODUCTION

II-VI compounds, CdTe and $Cd_{0.9}Zn_{0.1}Te$ (CZT) are by far the most suitable semiconductor materials for room temperature x- and gamma ray detectors.[1,2] Because of high Z composition, CZT provides high gamma-ray absorption cross-section even for small volume detectors. CZT also has the pre-requisite detection properties like low leakage currents at high operating bias voltages, wide band gap (>1.5 eV at 300 K), high density (5.8 g/cm^3), which invariably made it a very suitable candidate for room-temperature nuclear radiation detection in the field of Homeland security, infrared focal plane arrays, space astronomy, environmental monitoring, and medical imaging applications.[3–11]

Even with the advent of better crystal quality, CZT based materials suffer from poor charge-transport properties, especially due to holes. Presence of various kinds of defects is thought to be responsible for trapping of holes. Macroscopic defects such as cracks and twin/grain boundaries and microstructural defects such as mosaic structures, tilt boundaries, dislocations, point defects, impurities, tellurium inclusions/precipitations often lead to poor transport properties in CZT materials.[1] In order to deal with poor hole-transport properties, several special detector geometries, e.g., virtual Frisch grid configuration,[12,13] coplanar grid structure,[14] and small pixel geometry[15] have been suggested till date, which render the detector as a single polarity charge sensing (electron in this case) device thus effectively eliminating the adverse effects of hole movement. Virtual Frisch grid devices are preferred to other configurations because of their effective single polarity sensing property, operational simplicity, and ease of fabrication. Among all virtual Frisch grid configuration, non-contacting Frisch collar maintains the single polarity nature of the detector with minimal leakage current between the anode and the grid as the Frisch collar is electrically isolated from the crystal surface.[13] Figure 1 shows a simplified weighting potential distribution (induced charge on an electrode) in an actual Frisch grid configuration, which implies that there would not be any induced charge on the anode unless the charge carriers are in the measurement region. Similar weighting potential distribution can be achieved using a virtual Frisch grid arrangement. However, in practice, the weighting field distribution may not be as well defined as shown in the figure and the detector may still suffer from the poor hole

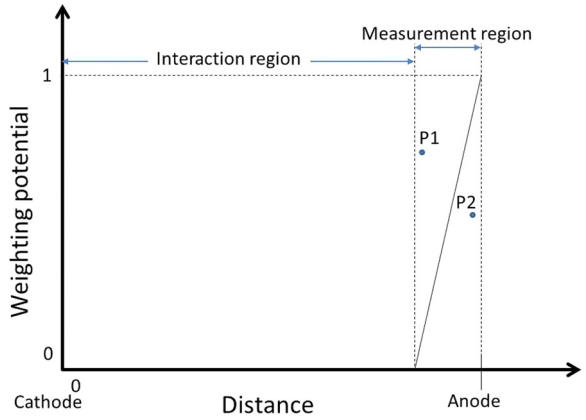

FIG. 1. Weighting potential distribution in a Frisch grid detector as a function of depth of interaction.

[a)]Author to whom correspondence should be addressed. Electronic mail: mandalk@cec.sc.edu. Tel.: +1-803-777-2722. Fax: 803-777-8045.

movement. Digital correction schemes such as biparametric correlation can be adopted in order to compensate for the effect of charge loss.[16]

In this article, we have fabricated and characterized two virtual Frisch grid detectors from detector grade CZT crystal grown using a Te solvent method and compared their performance as a high-energy gamma detector. Gamma ray spectroscopy using a ^{137}Cs source revealed well resolved 662 keV peaks. A biparametric correlation study involving the depth of interaction of the 662 keV gamma rays and the corresponding charge induced at the electrodes, revealed an anomalous pattern in the case of one of the detectors. The anomalous pattern has been explained by correlating the results obtained from thermally stimulated current (TSC) spectroscopy, which suggested that the behavior could be attributed to the effect of hole trapping in the interaction region modified by the virtual Frisch grid effect.

II. EXPERIMENTAL METHODS

A. Detector fabrication

Detector grade $Cd_{0.9}Zn_{0.1}Te$ crystals were grown from zone refined (ZR) Cd, Zn, and Te precursors (~7 N purity) using a tellurium solvent method. The details of the tellurium solvent method used here can be found elsewhere.[17,18] Crystals of various dimensions have been cut out from the grown ingot and, ground, lapped (down to 0.3 μm alumina) and polished (down to 0.3 μm diamond paste). The mechanically polished crystals were etched chemically using 1.5% Br_2/methanol solution for 60 s. Gold contacts (50-70 Å) were deposited on two opposite sides of the crystal using a sputtering unit. The virtual Frisch grid configuration was achieved with a copper sheath tightly wrapped around the crystal. The length of the copper collar covered the whole detector thickness. The collar was electrically insulated from the CZT material by lining the crystal side surfaces with insulating teflon tape. The approximate thickness of the insulating layer was 60 μm. The copper collar contained a projected tab, which was used to connect to the cathode. The physical dimensions of the two crystals used in this study were $4.2 \times 6.2 \times 6.5$ mm^3 for detector D1 and $3.0 \times 4.0 \times 9.0$ mm^3 for detector D2.

B. Detector characterization

The detectors were tested for their electrical characteristics using I-V measurements. The measurements were carried out using a Keithley 237 source-measure unit at room temperature. The detectors were placed in a light-tight RFI/EMI shielded test box during the measurements.

Gamma ray spectroscopic measurements were carried out at room temperature using an analog spectrometer. An Amptek A250CF preamplifier was used to collect the radiation induced charges in the detector. Before the actual measurements, the spectrometer was calibrated using a precision pulser. The bias-voltage and the amplifier shaping-time settings were optimized separately for each detector. The pulse-height spectra were acquired using a 5 μCi ^{137}Cs radioisotope. The detectors were irradiated at the cathode and the output signal was acquired at the anode, which was positively biased. The energy-resolutions of the detectors were measured in terms of the full width at half maxima (FWHM) of the full energy peak in the pulse-height spectra after a Gaussian fit of the relevant peak with proper baseline subtraction.

C. Digital spectroscopic measurements

A digital data acquisition system was set up using a high-speed and high-resolution NI digitizer card (PCI 5122) to digitize the pre-amplifier (A250CF) signals. A LABVIEW based data-acquisition software was developed to acquire and store the digitized pulses. Nearly 50 000 pulses were acquired for each run with a sampling rate of 100 MS/s and a 14 bit vertical resolution. A separate program was developed using LABVIEW and MATLAB codes to process and analyze the digitized data offline. The data analyses involved determination of pulse rise-times and digital semi-Gaussian (CR-RC^4) shaping of the pulses followed by pulse-height determination and biparametric correlation. The rise-times were calculated as the time interval to reach 90% of the maximum pulse-height from 10%. Biparametric correlation was obtained by mapping the depth of interaction of the gamma rays and the corresponding pulse-heights of the signal generated from those interactions. The depth of interaction was assumed to be proportional to the rise-time of the output charge pulses. Biparametric plots essentially reveal deviation from an ideal behavior of the detector. Noticed deviation from the ideal behavior, which leads to a broadening of the peaks, was corrected numerically using suitable correction factors. Finally, corrected pulse-height spectrum was regenerated from the corrected biparametric plot.

III. RESULTS AND DISCUSSIONS

A. I-V characteristics

Figure 2 shows the room-temperature I-V characteristics for detectors D1 and D2. The I-V characteristics were found to be nearly symmetric in the positive and the negative regimes, confirming the Ohmic nature of the gold contacts.

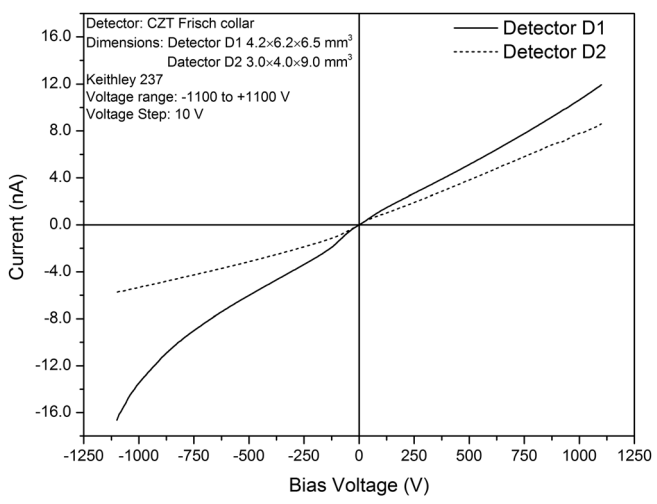

FIG. 2. Room temperature current-voltage characteristics of detectors D1 and D2 in virtual Frisch grid geometry.

The room-temperature leakage currents were found to be quite low at 1100 V, ~11 nA for detector D1, and ~8 nA for detector D2 confirming the high resistivity of the CZT crystals. The magnitude of leakage currents in detector D2 was found to be smaller compared to that in the detector D1 because of its smaller area and larger thickness. Detector D2 was biased further up to 1800 V in a separate measurement and the corresponding leakage current was found to be ~14.5 nA.

B. Gamma ray measurements

Figure 3 shows a ^{137}Cs gamma spectrum recorded using detector D1 biased at 1200 V. The full energy peak corresponding to the 662 keV gamma rays was seen to be clearly resolved and the other spectral features like the Compton edge and the backscattered peak were also distinctly visible. The full energy peak was fitted using a Gaussian function and the percentage resolution was calculated to be 1.6% (9.22 keV) with a peak-to-valley (P/V) ratio of 2.6. Figure 4 shows the spectral response of detector D2 biased at 1500 V and exposed to the ^{137}Cs gamma rays. It can be noticed that the detector D2 also showed well-resolved spectral features, e.g., the full energy peak, Compton edge, and the backscattered peak. However, the energy distribution of the full energy peak has an FWHM of 5.9% (29 keV), which is much broader compared to that obtained from detector D1. The peak-to-Compton ratio was found to be less than 1 and the centroid position of the full energy peak on the calibrated multi-channel analyser was found to be at around 500 keV instead of 662 keV. These are normally indicative of incomplete charge collection due to insufficient strength of the applied electric field or bias. Application of higher bias did not result in improved performance as the leakage current was seen to increase accordingly resulting in increase in parallel noise. However, it cannot be confirmed whether the poor resolution (or poor charge collection) observed in the case of detector D2 is due to the insufficient strength of the electric field or due to the trapping of charges in defect centres. Further insight into the problem can be gained with the help of digital spectroscopy where pulse by pulse analyses facilitate correlation of different pulse parameters from same events.

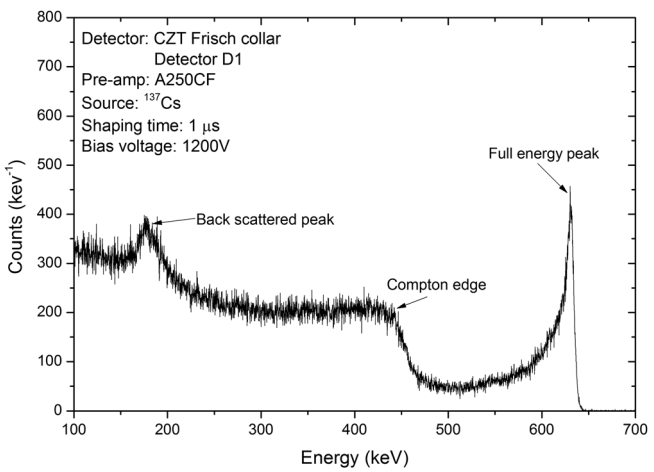

FIG. 3. ^{137}Cs pulse-height spectrum obtained using virtual Frisch grid detector D1.

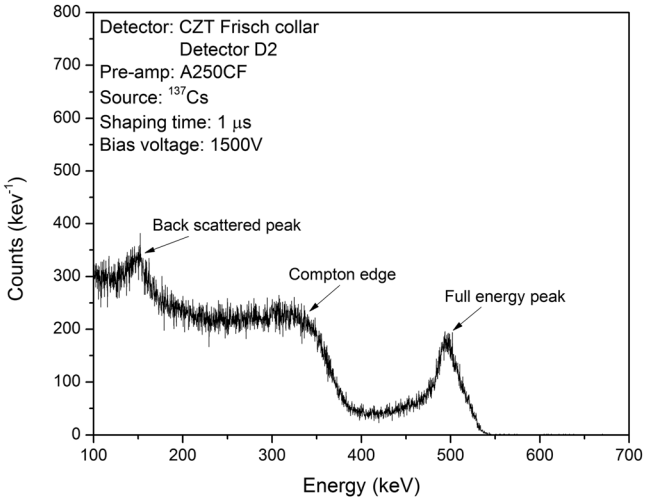

FIG. 4. ^{137}Cs pulse-height spectrum obtained using virtual Frisch grid detector D2.

Figures 5(a) and 5(b) show the 10%–90% rise-time distribution of the charge pulses generated from detectors D1 and D2, respectively, using a ^{137}Cs source. The rise-time of the signal pulses in planar detector geometry is directly proportional to the drift-time of the charge carriers from the point of interaction to the collecting electrode, i.e., the pulse rise-times can be considered equivalent to the drift-time of electrons plus that of the hole movement from the point of their generation. In the case of a virtual Frisch grid configuration, the rise-time of the pulses essentially gives the transit-time of electron movements in the measurement region. The average rise-time of pulses obtained from the centroid position of the rise-time distribution for the detector D1 was found to be less than that of detector D2, which implies that the weighting potential distribution is steeper in the measurement region in detector D1 compared to that in detector D2 resulting in a rapid transit of the electrons in this region. Also, a broader distribution of the rise-times in the

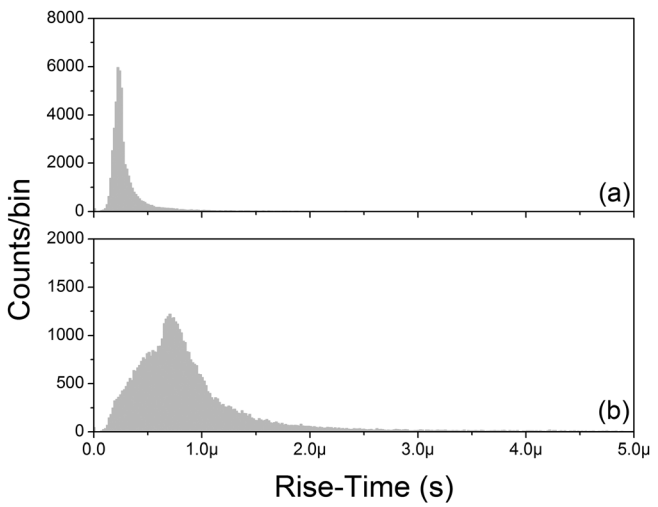

FIG. 5. Rise-time distribution of charge pulses obtained using a ^{137}Cs source for detector D1 (a) and detector D2 (b).

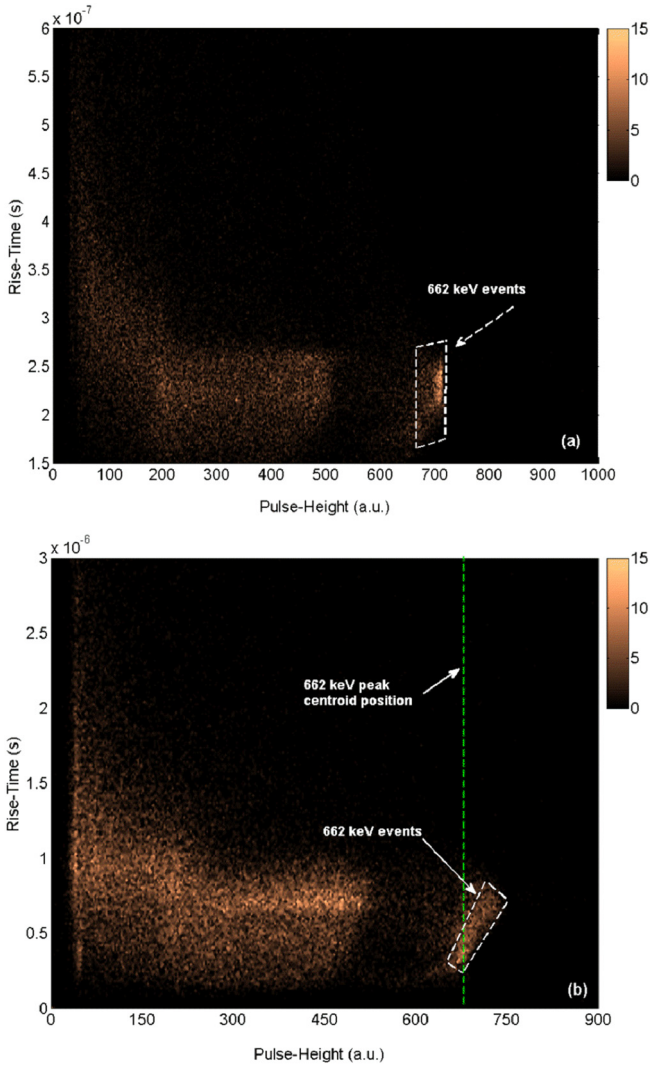

FIG. 6. Biparametric plot obtained using a ^{137}Cs source for detector D1 (a) and detector D2 (b).

case of detector D2 reflects the combined effect of trapping and incomplete charge collection on the detector output signal. The effect of rise-time distribution on the energy resolution can be understood from the biparametric plots.

Figures 6(a) and 6(b) show the biparametric correlation plot of the 662 keV interaction events obtained for the detectors D1 and D2, respectively. The plots are basically three-dimensional plots with the x-axis representing the pulse-heights, the y-axis representing the rise-time, and the number of events displayed by the graded color (black being low and white being high in grayscale picture). The 662 keV full-energy events marked by the dotted lines can be clearly distinguished from the Compton events in the biparametric plots. In an ideal defect free virtual Frisch grid detector with all the interactions taking place in the interaction region (see Fig. 1), a biparametric plot is expected to exhibit a narrow distribution of both rise-time and pulse-height. However, in our case, both the detectors were found to show a distribution in the rise-times of the 662 keV events. It can be further noticed from Fig. 6(a) that most of the 662 keV events, enclosed within the dotted lines, are aligned vertically with respect to the rise-time axis. Some of the events with less pulse-height compared to the 662 keV events could be seen scattered between the region of the Compton events and the full-energy 662 keV events. The origin of these events can be explained as follows. Given a random distribution of hole trapping centres within the detector thickness and the fact that gamma rays of a particular energy can interact anywhere within this thickness, signals with various rise-times and pulse-heights can be obtained for that particular energy. For the interactions close to the cathode, the electron movements form the major part of the signal, but for interactions close to the anode (collecting electrode in this case) hole movement contributes more to the signal. Due to their poor transport properties, the holes drift slowly compared to the electrons and hence the resulting signal has a higher rise-time. Moreover, the holes trapped in defect sites may eventually recombine resulting in a partial charge induction on the anode. So, the events for gamma rays with a particular energy may exhibit less pulse-height for interactions close to the cathode. In an ideal Frisch grid device, this effect is not expected as the charge-carrier is not "seen" by the collecting electrode unless it reaches the measurement region. However, in practice, the weighting potential distribution is not as well defined and steep as shown in Fig. 1, and hence pulse-height spectra can be affected by the charge loss. The distribution of the weighting field can vary depending on various factors such as dimensions of the crystal (aspect ratio), Frisch collar length, and thickness of the dielectric used to electrically isolate the collar from the crystal.[19] Verger *et al.*,[16] have shown similar effect of charge-loss and corresponding biparametric treatment in their virtual Frisch grid CZT detectors.

On the other hand, the 662 keV events in biparametric plot obtained for detector D2, shown in Figure 6(b), show an altogether different behavior. It can be seen that the 662 keV events were inclined towards the high energy side of the actual peak position, which is in contrast to the normal hole trapping signature (inclination to the left side), e.g., in planar detectors.[20] This atypical behavior can be still attributed to hole trapping and de-trapping effect and can be explained as follows. Let us consider two instances of position of interactions marked as P1 and P2 in Fig. 1. In the case of interactions at P2, the induced signals would be due to the combined electron-hole movement. The hole current will be affected by their trapping and de-trapping in the defect sites resulting in longer pulse rise-times. On the other hand, for the interactions at P1, the output signal will be primarily due to the electron movements. So the induced charge is expected to be less than that of combined charge induction from both electrons and holes and hence shows a lower pulse-height. Since the electron movements are comparatively faster, the rise-times will be smaller for these interactions.

Although the performance of CZT detectors is more affected by the poor hole movement than electrons, as is evident from the lower mobility and mobility-lifetime product of holes,[21] the effect of electron trapping cannot be ignored either. Table I shows a summary of the results of the TSC measurements carried out previously in this sample.[10] Schottky diodes were fabricated on CZT sister samples (samples from the same section of the ingot) by depositing

TABLE I. Defects and related parameters identified using TSC studies[10] in a sister CZT sample from the same section of the ingot.

Identified defects	Activation energy (eV)	Capture cross-section (cm^2)
$V_{Cd}^{0/-}$	0.18	10^{-19}–10^{-16}
$(Te_{Cd}^{+2}V_{Cd})^{2-/-}$	0.46	10^{-12}
$(Te_{Cd}^{+2}V_{Cd})^{3-/2-}$ or $(Te_{Cd}^{+}V_{Cd})^{-/0}$	0.86	…
$Te_{Cd}^{+2/+}$	0.58	4×10^{-14}
$Te_{Cd}^{0/+}$	0.26	10^{-18}
$V_{Cd}^{2-/-}$	0.27	10^{-15}

high purity indium followed by rapid thermal annealing at 550 K for 1 min in nitrogen ambience. The identified defects were found to be different charge states of the cadmium vacancies (V_{Cd}) and tellurium antisites (Te_{Cd}) or their complexes. The negatively charged defects were seen to dominate, e.g., the defect complex $(Te_{Cd}^{+2}V_{Cd})^{2-/-}$ showed the highest capture cross-section of 10^{-12} cm^2 among all other characterized defects and also the defect complexes $(Te_{Cd}^{+2}V_{Cd})^{3-/2-}$ and $(Te_{Cd}^{+}V_{Cd})^{-/0}$ were found to be in high concentration. Among the positively charged defects, $Te_{Cd}^{+2/+}$ was found to have a high concentration and a capture cross-section of 4×10^{-14} cm^2. So, the negatively charged defects or the hole traps are most likely to affect the detector performance, however, the trapping of electrons cannot be ignored either.

It would be worth discussing here that the effect of trapping could be seen to some extent in the case of detector D1, but it was negligible compared to the case of detector D2. One of the plausible reasons could be the higher defect concentration in the case of detector D2 leading to massive trapping. Although both the crystals were derived from the same grown ingot, it was found from an electron beam induced current (EBIC) measurements that there exists a non-uniformity in the spatial distribution of Te inclusions/precipitations.[10] It is also worth mentioning here that although the two detectors had different aspect ratios (defined as the ratio of the device length to the average device width), it was not thought to be a reason behind their different behavior. Kargar *et al.*[19] have shown that the detector performance even with the Frisch collar could not be improved if the geometrical aspect ratio is less than 1.5. In our case, the average aspect ratio of detector D1 is less than 1 and that of detector D2 is ~3. Following the finding of Kargar *et al.*,[19] detector D2 should have performed better if there was any effect due to the aspect ratio.

As a final step, a correction scheme was applied to the biparametric plot shown in Fig. 6(b) for the detector D2. Figure 7(a) shows the biparametric plot obtained after the correction. The events which were inclined with a positive slope were selectively aligned to the 662 keV line. The corrected pulse-height spectrum regenerated from the corrected biparametric plot was shown in Fig. 7(b). The photo-peak can be seen to have a narrower distribution with an FWHM of 3.13% and an improved peak-to-valley (P/V) ratio of 6.

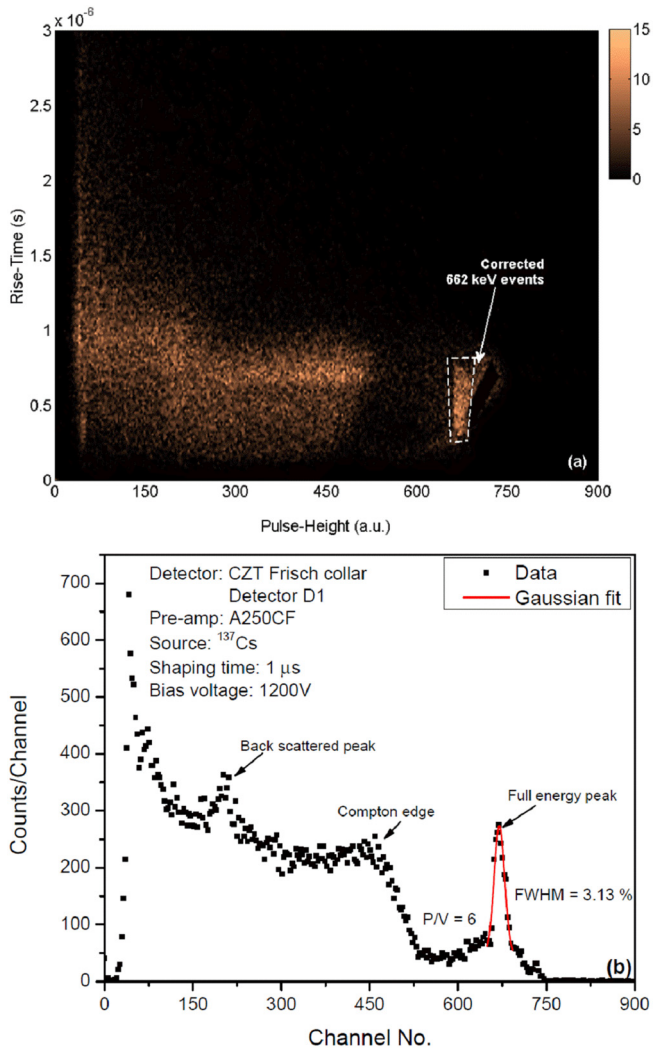

FIG. 7. (a) Biparametric plot obtained after correction for detector D2 and (b) the corresponding corrected pulse-height spectrum.

The corrected spectrum is partially recovered as is evident from the scattered events lying in the region between the Compton events and the full-energy events even after the correction. These events did not show any well-defined correlation and hence it was difficult to apply a correction scheme. These events could be, however, rejected to improve the pulse-height spectrum but at the cost of detection efficiency.

IV. CONCLUSIONS

Two virtual Frisch grid detectors have been fabricated and characterized from detector grade $Cd_{0.9}Zn_{0.1}Te$ single crystals grown using a tellurium solvent method. Although from the same ingot, the two detectors exhibited very different behavior when characterized using gamma radiations from a ^{137}Cs source. One of the detectors (D1) showed high energy resolution, narrow pulse rise-time distribution, and normal biparametric correlation plots. The other detector (D2) showed poor energy resolution, broad pulse rise-time distribution, and atypical biparametric behavior. Correlation of thermally stimulated current spectroscopic results and biparametric correlation analyses suggested that the atypical

biparametric behaviour of the detector D2 is due to the hole trapping effects in negatively charged deep level defects modified by the presence of the virtual Frisch grid. A biparametric correction scheme was applied to the case of detector D2 to partially recover the pulse-height spectrum from the charge trapping effects.

ACKNOWLEDGMENTS

This research was performed using partial funding received from the DOE Office of Nuclear Energy's Nuclear Energy University Programs (Grant No. DE-AC07-05ID14517).

[1]T. E. Schlesinger, J. E. Toney, H. Yoon, E. Y. Lee, B. A. Brunett, L. Franks, and R. B. James, Mater. Sci. Eng. R. **32**, 103 (2001).
[2]M. Niraula, K. Yasuda, S. Namba, T. Kondo, S. Muramatsu, H. Yamashita, Y. Wajima, and Y. Agata, IEEE Trans. Electron Devices **59**, 3450 (2012).
[3]U. N. Roy, A. Gueorguiev, S. Weiller, and J. Stein, J. Cryst. Growth **312**, 33 (2009).
[4]U. N. Roy, S. Weiller, J. Stein, M. Groza, V. Buliga, and A. Burger, IEEE Trans. Nucl. Sci. **58**, 1949 (2011).
[5]M. Groza, H. Krawczynski, A. Garson, J. W. Martin, K. Lee, Q. Li, M. Beilicke, Y. Cui, V. Buliga, M. Guo, C. Coca, and A. Burger, J. Appl. Phys. **107**, 023704 (2010).
[6]H. Chen, S. A. Awadalla, K. Iniewski, P. H. Lu, F. Harris, J. Mackenzie, T. Hasanen, W. Chen, R. Redden, G. Bindley, I. Kuvvetli, C. Budtz-Jørgensen, P. Luke, M. Amman, J. S. Lee, A. E. Bolotnikov, G. S. Camarda, Y. Cui, A. Hossain, and R. B. James, J. Appl. Phys. **103**, 014903 (2008).
[7]P. J. Sellin, Nucl. Instrum. Methods Phys. Res. A **513**, 332 (2003).
[8]A. E. Bolotnikov, J. Butcher, G. S. Camarda, Y. Cui, G. De Geronimo, J. Fried, R. Gul, P. M. Fochuk, M. Hamade, A. Hossain, K. H. Kim, O. V. Kopach, M. Petryk, E. Vernon, G. Yang, and R. B. James, IEEE Trans. Nucl. Sci. **59**, 1544 (2012).
[9]K. C. Mandal, S. H. Kang, M. Choi, A. Kargar, M. J. Harrison, D. S. McGregor, A. E. Bolotnikov, G. A. Carini, G. C. Camarda, and R. B. James, IEEE Trans. Nucl. Sci. **54**, 802 (2007).
[10]K. C. Mandal, R. M. Krishna, P. G. Muzykov, and T. C. Hayes, IEEE Trans. Nucl. Sci. **59**, 1504 (2012).
[11]H. Chen, S. A. Awadalla, F. Harris, L. Pinghe, R. Redden, G. Bindley, A. Copete, J. Hong, J. Grindlay, M. Amman, J. S. Lee, P. Luke, I. Kuvvetli, and C. Budtz-Jorgensen, IEEE Trans. Nucl. Sci. **55**, 1567 (2008).
[12]D. S. McGregor, Z. He, H. A. Seifert, D. K. Wehe, and R. A. Rojeski, Appl. Phys. Lett. **72**, 792 (1998).
[13]W. J. McNiel, D. S. McGregor, A. E. Bolotnikov, G. W. Wright, and R. B. James, Appl. Phys. Lett. **84**, 1988 (2004).
[14]P. N. Luke, Appl. Phys. Lett. **65**, 2884 (1994).
[15]H. H. Barrett, J. D. Eskin, and H. B. Barber, Phys. Rev. Lett. **75**, 156 (1995).
[16]L. Verger, J. P. Bonnefoy, F. Glasser, and P. Ouvrier-Buffet, J. Electron. Mater. **26**, 738 (1997).
[17]R. M. Krishna, T. C. Hayes, P. G. Muzykov, and K. C. Mandal, Mater. Res. Soc. Symp. Proc. **1341**, 39 (2011).
[18]R. M. Krishna, P. G. Muzykov, and K. C. Mandal, J. Phys. Chem. Solids **74**, 170 (2013).
[19]A. Kargar, A. C. Brooks, M. J. Harrison, K. T. Kohman, R. B. Lowell, R. C. Keyes, H. Chen, G. Bindley, and D. S. McGregor, IEEE Trans. Nucl. Sci. **56**, 824 (2009).
[20]S. K. Chaudhuri, A. Lohstroh, M. Nakhostin, and P. J. Sellin, J. Instrum. **7**, T04002-1-13 (2012).
[21]A. Owens and A. Peacock, Nucl. Instrum. Methods Phys. Res. A **531**, 18 (2004).